Crystal structure of a far-red–sensing cyanobacteriochrome reveals an atypical bilin conformation and spectral tuning mechanism

Sepalika Bandara[a,1], Nathan C. Rockwell[b,1], Xiaoli Zeng[a,1], Zhong Ren[a], Cong Wang[a], Heewhan Shin[a], Shelley S. Martin[b], Marcus V. Moreno[b], J. Clark Lagarias[b,2], and Xiaojing Yang[a,c,2]

[a]Department of Chemistry, University of Illinois, Chicago, IL 60607; [b]Department of Molecular and Cellular Biology, University of California, Davis, CA 95616; and [c]Department of Ophthalmology and Vision Sciences, University of Illinois, Chicago, IL 60607

Contributed by J. Clark Lagarias, February 2, 2021 (sent for review December 5, 2020; reviewed by Yuu Hirose and Hugo Scheer)

Cyanobacteriochromes (CBCRs) are small, linear tetrapyrrole (bilin)-binding photoreceptors in the phytochrome superfamily that regulate diverse light-mediated adaptive processes in cyanobacteria. More spectrally diverse than canonical red/far-red–sensing phytochromes, CBCRs were thought to be restricted to sensing visible and near UV light until recently when several subfamilies with far-red–sensing representatives (frCBCRs) were discovered. Two of these frCBCRs subfamilies have been shown to incorporate bilin precursors with larger pi-conjugated chromophores, while the third frCBCR subfamily uses the same phycocyanobilin precursor found in the bulk of the known CBCRs. To elucidate the molecular basis of far-red light perception by this third frCBCR subfamily, we determined the crystal structure of the far-red–absorbing dark state of one such frCBCR Anacy_2551g3 from *Anabaena cylindrica* PCC 7122 which exhibits a reversible far-red/orange photocycle. Determined by room temperature serial crystallography and cryocrystallography, the refined 2.7-Å structure reveals an unusual *all-Z,syn* configuration of the phycocyanobilin (PCB) chromophore that is considerably less extended than those of previously characterized red-light sensors in the phytochrome superfamily. Based on structural and spectroscopic comparisons with other bilin-binding proteins together with site-directed mutagenesis data, our studies reveal protein–chromophore interactions that are critical for the atypical bathochromic shift. Based on these analyses, we propose that far-red absorption in Anacy_2551g3 is the result of the additive effect of two distinct red-shift mechanisms involving cationic bilin lactim tautomers stabilized by a constrained *all-Z,syn* conformation and specific interactions with a highly conserved anionic residue.

bilin-based photoreceptor | optogenetics | serial crystallography | far-red-light sensing | bilin tautomers

Cyanobacteria have developed elaborate, spectrally tuned photoreceptors and light-harvesting systems for adaptation and survival in a wide range of ecological niches (1–5). Many photoreceptor systems are modular components of much larger signaling proteins that integrate different sensor and effector modules into a single protein molecule to interface with diverse signal transduction pathways. Photoreceptors in the phytochrome superfamily utilize a specific lineage of GAF (cGMP phosphodiesterase, adenylyl cyclase and FhlA) domain that binds a thioether-linked linear tetrapyrrole (bilin) chromophore for light perception (6–11). Bilin-based photoreceptors play critical roles in plant development as well as in regulating cyanobacterial phototaxis, development, and light harvesting (2, 3, 12–17). Protein structural changes following the primary photochemical event then alter the downstream enzymatic activities and/or protein–protein interactions via an interdomain allosteric mechanism (18).

Phytochromes possess a tripartite photosensory region consisting of three N-terminal domains (PAS, GAF, and PHY), known as the photosensory core module, in which the PAS and GAF domains are tethered via a "figure-eight knot" (14, 19, 20). In prototypical phytochromes, the bilin chromophore embedded in the GAF domain adopts a protonated *5-Z,syn*, *10-Z,syn*, *15-Z,anti* configuration in the dark-adapted state. Light absorption triggers photoisomerization of the 15,16 double bond to generate a *15E,anti* photoproduct, which typically absorbs far-red light (9, 14, 21). A long extension from the adjacent PHY domain is responsible for stabilizing the far-red–absorbing Pfr state (14, 20). In cyanobacteria, the phytochrome superfamily has diversified to yield a large family of more streamlined sensors, designated cyanobacteriochromes (CBCRs) (2, 4, 22–26). Unlike canonical phytochromes, CBCR photosensory modules consist of one or more GAF domains that are sufficient for covalent attachment of bilin and photoconversion. These small CBCR domains have also been used as light-sensing modules in a variety of synthetic biology applications (27–32). In contrast to canonical red/far-red phytochromes, CBCRs are able to sense light from near UV to far-red, utilizing a common phycocyanobilin (PCB) chromophore precursor (22–24, 26).

The remarkable spectral diversity of CBCRs (*SI Appendix*, Fig. S1*A*) arises from extensive molecular evolution of the GAF domain scaffold. Many CBCRs leverage two thioether linkages to sense blue, violet, or near-UV light (8, 22, 23, 25, 33–35). Such "two-Cys" CBCRs possess an additional thioether linkage to the C10 methine bridge of the bilin that splits the chromophore in half, significantly shortening the conjugated π-system. Rupture of

Significance

Phytochromes are well-known far-red-light sensors found in plants that trigger adaptive responses to facilitate competition for light capture with neighboring plants. Red- and far-red sensing are also critical for cyanobacteria living in the far-red–enriched shade of plants. This work reports the crystal structure of a far-red–sensing cyanobacteriochrome, a distant cyanobacterial relative of phytochrome. These studies shed insights into the molecular basis of far-red-sensing by phycobilin-based photoreceptors. Owing to the deep tissue penetration of far-red light, far-red–sensing cyanobacteriochromes are promising protein scaffolds for developing genetically encoded photoswitches, optoacoustic contrast agents, and fluorescent probes for in situ imaging and optogenetic applications.

Author contributions: S.B., J.C.L., and X.Y. designed research; S.B., N.C.R., X.Z., Z.R., C.W., H.S., S.S.M., M.V.M., and X.Y. performed research; S.B., N.C.R., M.V.M., J.C.L., and X.Y. analyzed data; and S.B., N.C.R., J.C.L., and X.Y. wrote the paper.

Reviewers: Y.H., Toyohashi University of Technology; and H.S., Universität München.

The authors declare no competing interest.

[1]S.B., N.C.R., and X.Z. contributed equally to this work.

[2]To whom correspondence may be addressed. Email: jclagarias@ucdavis.edu or xiaojing@uic.edu.

This article contains supporting information online at https://www.pnas.org/lookup/suppl/doi:10.1073/pnas.2025094118/-/DCSupplemental.

Published March 16, 2021.

this covalent bond can occur upon *15Z*/*15E* photoisomerization, which restores bilin conjugation across C10 to generate a photostate absorbing at wavelengths from teal to red (8, 33, 36, 37). Dual cysteine CBCRs have evolved multiple times, yielding a wide range of photocycles with (ultra)violet, blue, teal, green, orange, and red states (22).

Red/green CBCRs such as AnPixJg2 and NpR6012g4 have red-absorbing dark states similar to phytochromes that photoconvert to green-absorbing lit states. In this CBCR subfamily, the molecular mechanism responsible for photoproduct tuning relies on trapping the *15E* bilin in a twisted geometry that results in blue-shifted absorption (10, 11). In contrast, green/red CBCRs exhibit a reversed photocycle: the green-absorbing *15Z* dark state photoconverts to yield a red-absorbing *15E* photoproduct. This subfamily uses a protochromic mechanism first reported for the light-regulated histidine kinase RcaE (*SI Appendix*, Fig. S1*B*) in which photoconversion triggers a proton transfer to an uncharged chromophore inducing a spectral red shift (2, 38).

Until recently, the light-sensing range of CBCRs appeared limited to the visible spectrum, thereby implicating phytochromes to be exclusively responsible for far-red sensing in cyanobacteria. Indeed, far-red–dependent remodeling of the photosynthetic apparatus in multiple cyanobacterial species is mediated by the red/far-red phytochrome RfpA (3, 39). The discovery of two lineages of CBCRs with far-red-absorbing dark states (frCBCRs) was thus surprising (40). Upon far-red light absorption, these frCBCRs convert to either an orange- or red-absorbing photoproduct state. These frCBCRs evolved from green/red CBCRs as part of a greater green/red (GGR) lineage and independent from evolution of other frCBCRs within the XRG (extended red/green) lineage (35, 40, 41). Owing to their small size and spectral overlap with the therapeutic window of optimum tissue penetrance (700 to 800 nm) (42–46), frCBCRs represent tantalizing scaffolds for development of FR-responsive optogenetic reagents for biomedical research and imaging applications (45, 47–50).

To understand the molecular basis of far-red spectral tuning of the frCBCR family that evolved within GGR lineage, we determined the crystal structures of the FR-absorbing dark state of the representative FR/O CBCR Anacy_2551g3 from *Anabaena cylindrica* PCC 7122 at both ambient and cryogenic temperatures. These structures revealed an *all-Z,syn* configuration of its PCB chromophore that differs from those found in all known CBCRs and phytochromes. Based upon these crystallographic results, spectra of site-directed mutants of Anacy_2551g3 and related frCBCRs in the GGR lineage, and comparisons with other bilin-binding proteins, we identify key protein–chromophore interactions that support two tuning mechanisms simultaneously at work for far-red light detection in this family of frCBCRs.

Results and Discussion

Crystal Structure of 2551g3 Reveals an Atypical *All-Z,syn* Chromophore. We have determined the structure of a representative frCBCR Anacy_2551g3 (hereafter, 2551g3) (40). The 2551g3 is the third GAF domain of a multidomain sensor histidine kinase encoded by locus Anacy_2551 from *A. cylindrica* PCC 7122 (*SI Appendix*, Fig. S1*B*). A truncated GAF-only construct of 2551g3 covalently incorporates PCB when coexpressed with a PCB-producing plasmid in *Escherichia coli* (40, 51, 52) and reversibly photoconverts between a FR-absorbing *15Z* dark state (Pfr; λmax 728 nm) and an orange-absorbing *15E* lit state (Po; λmax 588 nm; *SI Appendix*, Fig. S2*A*). The crystal structure of 2551g3 in its Pfr dark state was determined at both cryogenic and room temperatures (Fig. 1 and *SI Appendix*, *Materials and Methods*). Retention of the Pfr state in the crystal was confirmed by single-crystal absorption spectroscopy and by the characteristic green color of 2551g3 crystals (*SI Appendix*, Fig. S2*B*). Monochromatic datasets collected at 100 K were used to obtain an initial model for 2551g3 at 3.1-Å resolution by the molecular replacement method (PHENIX) using the

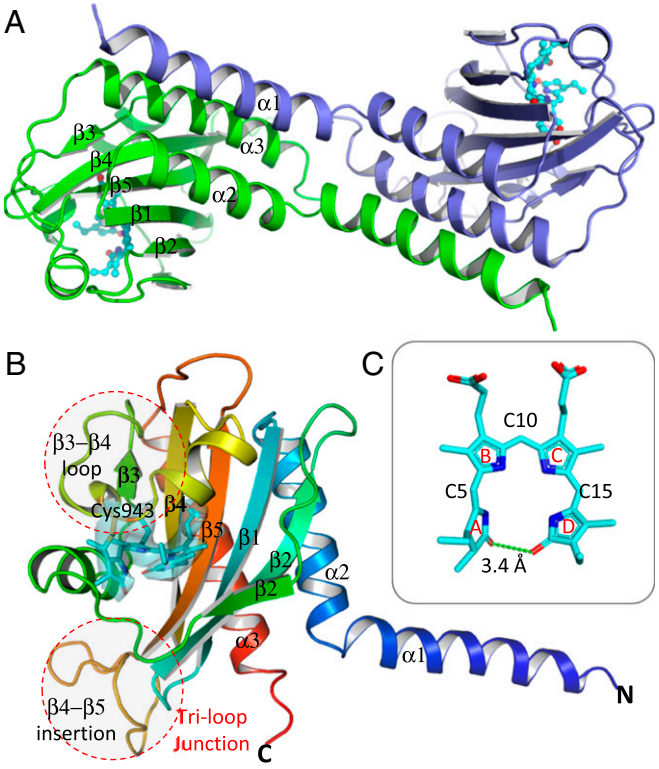

Fig. 1. Crystal structure of far-red CBCR 2551g3 in the Pfr state. (*A*) In a handshake dimer structure of 2551g3, the GAF-α1 helix of one protein molecule (green) extends out to form a three-helix bundle with the GAF-α2 and GAF-α3 helices from the partner molecule (blue). (*B*) Phycocyanobilin (PCB; cyan) is located in a cleft sandwiched by the β3–β4 and β2–β3 linkers. The electron densities of the 2Fo-Fc map (rendered in transparent cyan surface at the 2.2σ contour) are shown for PCB and the Cys943 anchor. Two structural features unique to the frCBCR family, a disjointed helix at the α-face and tri-loop junction at the β-face, are highlighted in red circles. (*C*) The PCB chromophore adopts an unusual *all-Z,syn* conformation.

two-Cys CBCR TePixJ crystal structure (PDB: 4GLQ) (8) as a search model. To improve the resolution and map quality, we employed an in situ room-temperature (RT) data collection method developed by our laboratory (53, 54), which yielded a complete Laue dataset at 2.7-Å resolution from >800 crystals. This serial RT crystallography strategy not only alleviates X-ray radiation damage but also evades crystal freezing, particularly beneficial given a high solvent content of ~70% in 2551g3 crystals. The resulting high-quality electron density map allowed us to build a complete 2551g3 structure with no gaps in the protein backbone. Compared to the cryocrystallography data, this RT structure shows excellent statistics both in the real space and reciprocal space (*SI Appendix*, Table S1) with well-resolved electron density for the bilin chromophore (Fig. 2*A*). Unless mentioned otherwise, the RT structure of 2551g3 is used for depiction and discussion in this work.

The Pfr structure of 2551g3 in the $P4_222$ space group contains one protein molecule in an asymmetric unit (Fig. 1). The core GAF domain features a typical α/β fold with a central β-sheet consisting of five β-strands in a topological order of β3–β4–β5–β1–β2 (Fig. 1*B*). A short β-strand labeled β2′, that lies within the linker region between β1 and β2, occupies the position of a sixth β-strand often found in canonical GAF domains. The GAF-α1 helix disengages from its own protomer and bundles with the GAF-α2 and GAF-α3 helices from a symmetry-related protomer, forming a "handshake" crystallographic dimer (Fig. 1*A*). The 2551g3 and related CBCRs are characterized by a large insertion between the β4 and β5 strands (amino acids 964 to 980) (40),

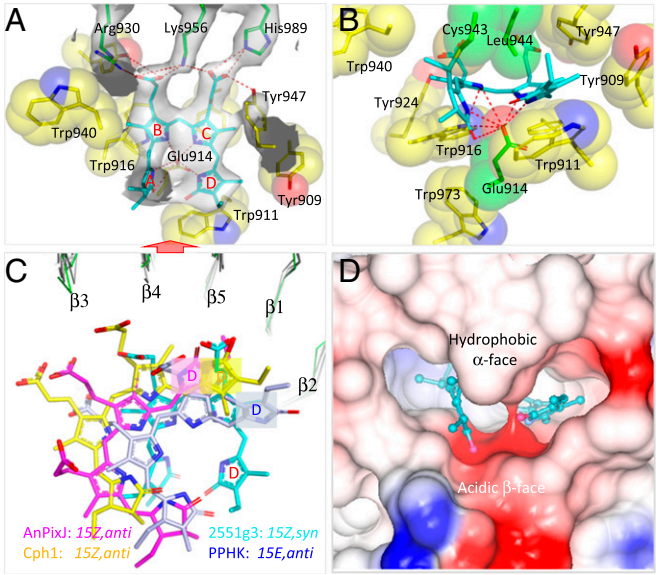

Fig. 2. The chromophore binding pocket in the Pfr structure of 2551g3. (*A*) The 2*Fo-Fc* map (contoured at 1.7 σ; rendered in gray transparent surface) shows close interactions between the propionates of PCB (cyan) and its protein anchors (Arg930/Lys956, His989/Tyr947; in green sticks). Distances between the carboxylate of Glu914 and four N atoms in pyrrole rings A, B, C, and D are 3.0, 3.4, 2.7, and 3.0 Å, respectively. (*B*) Viewed from the red arrow in *A*, Leu944 is located next to the Cys943 anchor at the α-face, whereas both rings A and D point toward the β-face. Red dashed lines highlight the hydrogen bonds between PCB and the acidic side chain of the hallmark residue Glu914. Yellow spheres mark the surrounding aromatic residues. (*C*) PCB in the Pfr structure of 2551g3 (cyan) assumes a distinct disposition relative to other phytochrome systems: canonical phytochrome Cph1 (2VEA: yellow), red/green CBCRs AnPixJ (3W2Z: magenta), and PPHK (6OAP: light blue). All structures are aligned based on the GAF protein framework (shown in thin wires). (*D*) The electrostatic surface in the PCB cavity is highly asymmetric between the α- and β-faces.

which contrasts with a tight turn typically found in other CBCRs and prokaryotic phytochromes (*SI Appendix*, Fig. S3*A*). This large insertion folds back toward the core and directly interacts with the β2–β3 linker and the β1–β2 loop, constituting a "tri-loop junction" structure located on the β-face of the chromophore (55) (Fig. 1*B*). On the α-face of PCB, two short helices in the β3–β4 linker are connected by a sharp turn containing Cys943, the conserved Cys to which the chromophore is covalently attached. This region differs from that of phytochromes and CBCRs where the Cys anchor is located at the start of a continuous three-turn helix (*SI Appendix*, Fig. S3*B*).

The chromophore pocket of 2551g3 is surrounded by aromatic residues conserved in other CBCRs (Fig. 2 *A* and *B*, yellow). The β3–β4 and β2–β3 linkers, respectively located at the α- and β-faces of the bilin, form a cleft that shields the chromophore (Fig. 1*B*). The PCB chromophore, which is attached to Cys943 via a thioether linkage to the ring A ethylidene group, adopts a compact *all-Z,syn* configuration. In this "cyclic" conformation, rings A and D tilt toward the β-face with respect to the plane of rings B and C (Fig. 1 *B* and *C*). The A and D ring planes are nearly perpendicular to each other with two carbonyl oxygen atoms separated by ∼3.4 Å (Fig. 1*C*). This *all-Z,syn* configuration also adopts anomalous dihedral angles about the C5 and C15 methine bridges when compared to 156 bilin-binding protein structures in the Protein Data Bank (*SI Appendix*, Fig. S4). The 2551g3 chromophore also assumes a much more distorted conformation compared to other *all-Z,syn* bilins bound to proteins such as the ferredoxin-dependent bilin reductase (FDBR) PcyA and the bilin lyase CpcT (*SI Appendix*, Fig. S5) (56, 57). In contrast, covalently attached bilins found in previously characterized phytochromes, CBCRs, and light-harvesting phycobiliproteins adopt extended *15-Z,anti* or *15-E,anti* configurations (7, 8, 10, 11, 14, 19, 20, 58, 59), which would cause major steric clashes with the chromophore binding pocket in 2551g3 (*SI Appendix*, Fig. S6). These clashes are in part reconciled in 2551g3 by clockwise rotation of the chromophore in the approximate plane of the bilin ring system when viewed from the chromophore α-face. To our best knowledge, ring D of the *all-Z,syn* bilin in 2551g3 assumes the most extreme clockwise orientation relative to the GAF framework among known phytochromes and CBCRs (Fig. 2*C*).

The *All-Z,syn* Bilin Engages Unique Protein–Chromophore Interactions. The 2551g3 structure reveals several unique protein–chromophore interactions in frCBCRs and related CBCRs (*SI Appendix*, Fig. S1*C*). First, Leu944 next to the anchor Cys943 replaces a histidine residue highly conserved in the phytochrome superfamily (Fig. 2*B*) (40). The hydrophobic Leu944 approaches the bilin from a disjointed α-facial helix, resulting in tilting of rings A and D toward the acidic β-face (Fig. 2 *B* and *D*). This creates a highly asymmetric protein environment for the chromophore, where the bilin oxygen atoms in both the rings A and D point toward the negatively charged β-face (Fig. 2*D*). Second, aromatic residues conserved in this frCBCR subfamily play a steric role in generating a snug protein pocket of 2551g3 where all bilin rings are constrained in the *all-Z,syn* conformation (40) (Fig. 2 *A* and *B*). Rings B and C are laterally clamped between Ile939/Trp940 and Tyr924 while engaging close steric interactions with Tyr916, Leu944, Phe884, and Tyr947 on both α- and β-faces. Ring D is stacked against Trp911, a position often occupied by an aromatic residue in this frCBCR family and related CBCRs (*SI Appendix*, Fig. S1*C*). Such steric effects preclude binding of any bilins in the more extended *15,anti* conformation (*SI Appendix*, Fig. S6). Third, the hallmark residue Glu914 on the β-face engages all four pyrrole nitrogen atoms in hydrogen bonding interactions with the longest distance to ring B and shorter distances to ring C and D, which is also evidenced by connectivity of the electron density map in this region (Fig. 2*A*). Forced to tilt toward the β-face by Leu944, ring A is also stabilized by β-facial NH hydrogen bonds with both Glu914 and Trp916 side chains (3.1- and 3.3-Å distances) and by apparent hydrogen bonding interactions to the carbonyl oxygen with the backbone NH and carbonyl groups of Lys915 (2.8- and 3.2-Å distances). In addition, the A ring carbonyl is located nearly equidistant from the D ring carbonyl and the carboxylate side chain of Glu914 (3.4 and 3.5 Å, respectively).

In addition to these steric and pyrrole orientation constraints, the bilin propionates engage ionic interactions with basic residues deep within the GAF β-sheet. Specifically, Arg930 and Lys956 form salt bridges with the ring B propionate, while His989, Tyr947, and Lys956 are well positioned to interact with the ring C propionate (Fig. 2*A* and *SI Appendix*, Fig. S3*C*). The electron densities associated with the ringC-His989 and ringC-Lys956 interactions are visible in the *2Fo-Fc* map of 2551g3 contoured above 3σ (Fig. 2*A*). In phytochromes and CBCRs, a polar residue at the equivalent position of His989 is important both for stabilizing the ring D in the *15Z,anti* conformation (7, 8, 10, 19, 20) and for interacting with the ring C propionate in the *15E,anti* conformation as seen in *Pa*BphP (14, 21) (*SI Appendix*, Fig. S6). In frCBCRs, the interaction between His989 and an extended C ring propionate plays a role in stabilizing the compact *all-Z,syn* chromophore.

Critical Residues for Far-Red Sensing Identified by Mutagenesis. To identify key protein–chromophore interactions for far-red absorption, we carried out site-directed mutagenesis on both 2551g3 and a closely related frCBCR Anacy_4718g3 (hereafter, 4718g3; *SI Appendix*, Fig. S1*B*) (40). A total of 34 variant proteins with substitutions occurring at 25 different positions were evaluated. Twenty of these exhibited a range of severe phenotypes including loss of bilin binding, loss of the far-red state, and major changes in

photoproduct tuning (*SI Appendix*, Fig. S7). The other 14 variants exhibited only slightly altered peak wavelengths and/or photoproduct lineshapes. Among the 9 variants that failed to bind bilin were single Leu substitutions for His989, Lys956, Arg930, and Asp938, which are residues directly involved in anchoring the bilin propionates (Fig. 2*A* and *SI Appendix*, Fig. S8*A*). The L944H variant of 2551g3, which restores the α-facial His residue typically found at the equivalent position in phytochromes and CBCRs, did not bind bilin either. It is possible that the slightly bulkier side chain of His prevents proper binding or attachment of the *all-Z,syn* bilin due to steric effects. However, the strikingly blue-shifted L1383N variant of 4718g3 at the same position retained PCB binding, but at a reduced level (*SI Appendix*, Fig. S7).

Aside from the L1383N variant of 4718g3, variants of two of three β-facial acidic residues altered far-red absorption of the dark state (*SI Appendix*, Figs. S7 and S8). One of them is the photoinactive E914D variant of 2551g3 that showed a blue-shifted dark state but bound chromophore poorly. The equivalent E1353Q and E1353D variants of 4718g3 failed to bind PCB, suggesting a critical role for this conserved β-facial glutamate residue (Glu914 for 2551g3) in both bilin binding and spectral tuning. Substitution of the adjacent Asp913 for Leu resulted in yet a larger blue shift, again with reduced chromophorylation. Not strictly conserved among frCBCRs, Asp913 forms a salt bridge to Arg972 and to Lys915 at the tri-loop junction in the 2551g3 structure. The R972A variant (R1410A of 4718g3), however, retained both far-red absorption and photoconversion (*SI Appendix*, Figs. S7 and S8), suggesting that the Lys915–Asp913 interaction (or conservative substitutions at these sites) support far-red tuning. The wild-type spectral properties of the E912N variant (D1351N of 4718g3) suggests that this acidic residue is not directly involved in spectral tuning. Taken together, these studies suggest that the hallmark residues L944 and Glu914 located respectively at the α- and β-face of the chromophore are critically important for maintaining the far-red–absorbing state in this family of frCBCRs.

Eight variants had normal far-red–absorbing dark states but exhibited photoproducts with red-shifted absorption maxima compared to the Po state of WT (*SI Appendix*, Fig. S7). These include single mutations of several bulky residues specific to this family of frCBCRs. Some of these variants showed abnormal far-red/red photocycles, whereas others exhibited mixtures of red- and orange-absorbing photoproducts (*SI Appendix*, Fig. S7*C*). Substitutions at Trp911 had variable effects: the W911L variant exhibited only minor effects on spectral tuning in 2551g3, while the equivalent W1350A and W1350F variants of 4718g3 as well as the W911F variant of 2551g3 exhibited red-shifted photoproduct states. Far-red/red photocycles were also seen in the W940L variant of 2551g3 and the corresponding W1379L variant of 4718g3, the I939P variant of 2551g3, and the corresponding I1378P variant of 4718g3 as well as the S917P/Q918P variant of 2551g3. On the other hand, mixed *15E* photoproducts were observed with substitutions at Tyr947 and the equivalent Tyr1386 of 4718g3 (*SI Appendix*, Fig. S7*C*). We note that the wild-type 4718g3 also exhibited a small amount of a red-absorbing photoproduct species as a shoulder (*SI Appendix*, Fig. S7*B*).

Overall, the Pfr dark state was largely retained in the Trp variants (*SI Appendix*, Fig. S7), suggesting that these signature Trp residues (*SI Appendix*, Fig. S1*C*) are not critical for far-red tuning of frCBCRs. However, variants of these bulky residues had more influence on spectral properties of the photoproducts. These Trp residues facilitate formation of the Po photoproduct state, possibly by steric compression of the *15E* conformation of PCB or by eliminating water molecules in the chromophore pocket. With steric constraints removed by mutagenesis at these Trp positions, the *15E* chromophore could adopt a more relaxed conformation or additional water molecules might be retained to yield a red-absorbing photoproduct (40, 60).

frCBCRs within the GGR Lineage Retain a Protonated Far-Red–Absorbing State. The high sequence similarity between frCBCRs and green/red CBCRs (*SI Appendix*, Fig. S1*B*) raised the possibility that frCBCRs have a protochromic photocycle similar to that of the green/red CBCRs RcaE and CcaS in which the deprotonated green-absorbing *15Z* photostate chromophore becomes protonated in the *15E* photoproduct (2). We therefore carried pH titration experiments to examine the protonation state of frCBCRs. The Pfr state of 2551g3 was quite stable over a wide range of pH from 5 to 10 (Fig. 3*A*). At pH >10, we detected partial formation of an orange-absorbing state that was fully reversible by lowering the pH.

For comparison, we also examined two other frCBCRs in this family, i.e., Syn7502_01757 (hereafter, 01757) and WP_046814686 (hereafter, 0468g3), identified by an updated phylogenetic analysis (*SI Appendix*, Fig. S9*A*). Both represent early-diverging members in the frCBCR cluster to which 2551g3 and 4718g3 belong (40) (*SI Appendix*, Fig. S9*A*). As expected, both proteins exhibited far-red *15Z* photostates (*SI Appendix*, Fig. S9 *B* and *C*). In contrast to the orange-absorbing photoproducts seen in 2551g3 and 4718g3, 01757 generated a green-absorbing photoproduct, whereas 0468g3 exhibited a red-absorbing photoproduct (*SI Appendix*, Fig. S9 *B* and *C*). Photoconversion of acid-denatured photoproducts confirmed that both proteins underwent the 15,16-photoisomerization reaction (*SI Appendix*, Fig. S9*D*). Given the diversity of photoproducts observed in the frCBCR clade and those of 2551g3 and 4718g3 variants (*SI Appendix*, Figs. S7*C* and S8 *B* and *C*), we redesignate this frCBCR lineage as FR/X CBCRs (*SI Appendix*, Fig. S9*A*).

To examine the bilin protonation state in the far-red–absorbing dark states of 01757 and 0468g3, pH titration experiments were next performed. At pH 10, 0468g3 exhibited ~50% loss of far-red absorption with a clear absorption rise in the yellow-to-orange region (Fig. 3*B*). By comparison, 01757 exhibited nearly complete loss of the far-red band at pH 10—a change that was concomitant with appearance of a well-resolved band in the green-to-orange region (Fig. 3*C*). Denaturation measurements established that these pH-dependent changes were not due to an irreversible chemical change in the bilin chromophore structure or to loss of the *15Z* configuation (Fig. 3*D*). Moreover, the pH-dependent difference spectra were remarkably similar for all the frCBCRs tested despite their different photoproducts and the variability of their spectral pH dependence (Fig. 3 *E* and *F*).

Based on these and previous pH titration experiments, the *15Z* Pfr dark states of frCBCRs possess relatively high pK_a values (~9 to 11), which are comparable to those of *15E* Pfr photoproduct states' phytochromes, albeit much higher than those of both *15Z* Pg (pK_a 5.6) and *15E* Pr (pK_a 7.9) states of RcaE (2, 61–64). This likely reflects the strong H bonding and ionic interactions that stabilize the protonated *15Z* states of frCBCRs. In the *15E* Pr photoproduct state of RcaE, these interactions are much less extensive (65). Sequence alignment shows that RcaE possesses Phe residues at positions equivalent to Tyr947, Trp911, and Trp916 found in 2551g3 (*SI Appendix*, Fig. S1*C*), which contribute to its more "desolvated" chromophore environment. While the RcaE structure in the 15Z Pg dark state would help resolve this issue, our results indicate that the far-red–absorbing dark states of FR/X CBCRs possess predominantly protonated, cationic bilin ring systems at physiological pHs.

Far-Red–Absorbing Mechanisms in the FR/X CBCR Lineage. To understand the structural basis for far-red sensing, we compared the 2551g3 structure with those of other bilin-binding proteins that also absorb far-red light. These included the *15E* dark-adapted state of the bacteriophytochrome *Pa*BphP (14) and the substrate-bound I86D variant of ferredoxin-dependent bilin reductase PcyA (14, 66) (Fig. 4*A*). Although both possess biliverdin IXα (BV) instead of PCB, their far-red absorption is much too red shifted to be explained by the extra double bonds found in BV. The bound bilin in all three proteins is stabilized by a network of H bonds mediated by a highly conserved acidic residue, i.e., Glu914 in 2551g3 and Asp105

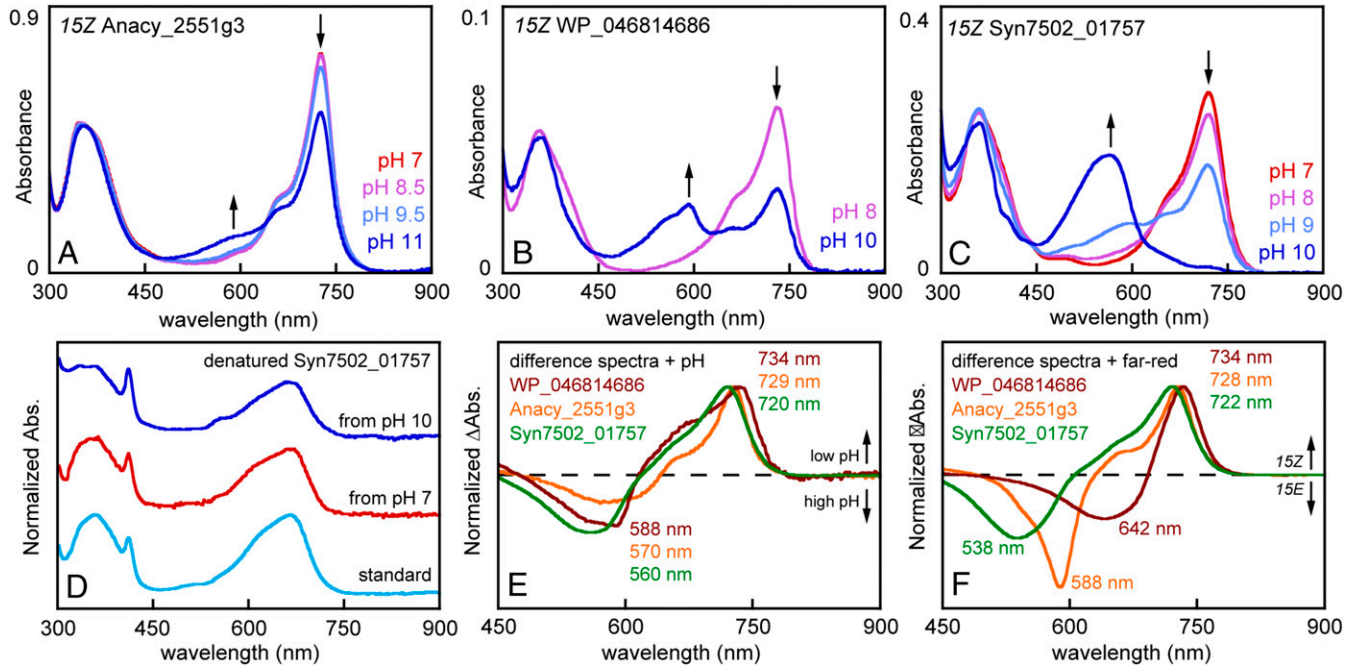

Fig. 3. pH titration experiments support a protonated chromophore in the far-red–absorbing state. (*A*) Absorbance spectra for *15Z* 4718g3 are shown at pH 7 (red) and pH 10 (dark blue). (*B*) Absorbance spectra for *15Z* 0468g3 are shown at pH 8 (mauve) and pH 10 (dark blue). (*C*) Absorbance spectra for *15Z* 01757 are shown at pH 7 (red), pH 8 (mauve), pH 9 (periwinkle), and pH 10 (dark blue). (*D*) Normalized absorbance spectra are shown for samples of *15Z* 01757 at standard pH 7.8 (teal), pH 7 (red), and pH 10 (dark blue) that were then denatured. (*E*) Normalized difference spectra are shown for *15Z* frCBCRs upon pH change: 2551g3 (orange, calculated from *A*), 0468g3 (brick red, calculated from *B*), and 01757 (green, calculated from extrema in *C*). (*F*) Normalized photochemical difference spectra are shown for 4718g3 (orange, calculated from *SI Appendix*, Fig. S7*B*, *Top*), 0468g3 (brick red, calculated from *SI Appendix*, Fig. S9*D*), and 01757 (green, calculated from *SI Appendix*, Fig. S9*B*).

in PcyA (56, 66), or Asp194 in *Pa*BphP (Fig. 4*A*). The more extended *5-Z,syn 10-Z,syn 15-E,anti* configuration of the BV chromophore in PaBphP contrasts with the cyclic *all Z-syn* chromophores of PcyA and 2551g3 (Fig. 4*A*), and PCB in 2551g3 displays a more twisted ring conformation compared to BV in PcyA (Fig. 4*B*). However, one structural feature is shared by all three proteins—the D ring nitrogen engages direct interaction with a highly conserved Glu or Asp residue, in which the carboxylic acid side chain presents an anionic counterion to the D ring NH group in a cationic bilin system that correlates with their far-red absorption.

We also observe a striking correlation between the Q band peak wavelength vs. pK_a of the residue interacting with the D ring NH group. In contrast to Glu/Asp in the far-red structures, Pr states of phytochromes and red/green CBCRs possess a much less acidic residue such as histidine or tyrosine that are hydrogen bonded with the D ring NH moiety of their *15Z,a* chromophores (Fig. 4*A*) (10, 20). The presence of an Arg residue next to the bilin NH moieties in the bilin lyase CpcT correlates with a green-absorbing CpcT–PCB complex in which PCB adopts an *all-Z,syn* conformation (Fig. 4*A*) (57). By comparison, the green-absorbing photoproduct states in red/green CBCRs PPHK and Slr1393 lack any hydrogen bond partner for ring D (67) (Fig. 4*A*). Although such comparisons between different systems with chemically distinct chromophores may not be ideal, these observations suggest that the presence of a negatively charged counterion near the D ring plays a critical role in far-red tuning. In this regard, recent excited-state calculations have supported the role of the Asp194–ring D interaction in conferring far-red absorption on the Pfr state of *Pa*BphP (68). We must also point out that this mechanistic hypothesis for far-red tuning in 2551g3 is at odds with a widely recognized tuning mechanism based on ring twist, that is, the less ring twist confers the longer peak wavelength (Fig. 4*C* and *SI Appendix*, Table S2) (10, 11, 69).

We therefore sought to reconcile the twisted PCB geometry of 2551g3 with its far-red absorption. In 2551g3, the *all,Z-syn* conformation is expected to lower the pK_a of bilin systems thereby disfavoring protonation of all four nitrogen atoms found in the more extended chromophores of phytochromes and most CBCRs. Using a model bilin molecule constrained in an *all,Z-syn* conformation, Krois showed that the fully protonated bilin exhibited a pronounced red-shifted absorption maximum and a pK_a lowered by 3 pH units (70). This investigator attributed this red-shifted species to a lactim isomer in which one of the bilin carbonyls is protonated, instead of protonation at all four bilin nitrogens as observed for the unconstrained bilins in solution. For this reason, far-red–absorbing protonated lactim species have been proposed as a model for the far-red–absorbing state of phytochromes, for example by Diller and coworkers (71).

For CBCRs and phytochromes, one can envisage two classes of bilin lactim isomers depending on whether the A or D ring oxygen atom is protonated. Each class has four possible tautomers varying in which of the four pyrrole nitrogen atoms is deprotonated (Fig. 5 and *SI Appendix*, Fig. S10). Interconversion between the four tautomers in each lactim isomer class is expected to be quite fast, while the equilibrium is largely influenced by the local protein environment. Although X-ray diffraction measurements at limited resolution do not reveal the precise locations of dissociable hydrogen atoms in 2551g3, we could infer their positions based on relative positions of proton donor/acceptor pairs, estimated pK_a values, protein environment, and chemical principles. Our interpretation is also informed by mutagenesis studies described earlier and by chromophore exchange experiments. With regard to the latter, a red-shifted native state of the frCBCR 4718g3 was consistently observed relative to the respective denatured state (40). Notably, the phycoerythrobilin (PEB) adduct of 4718g3, whose D ring is deconjugated from the ABC ring system as a result of its saturated C15 methine bridge, show the same trend as do the photoproduct states of all photoactive bilin adducts tested (40). Specifically, PEB in 4718g3 displayed an

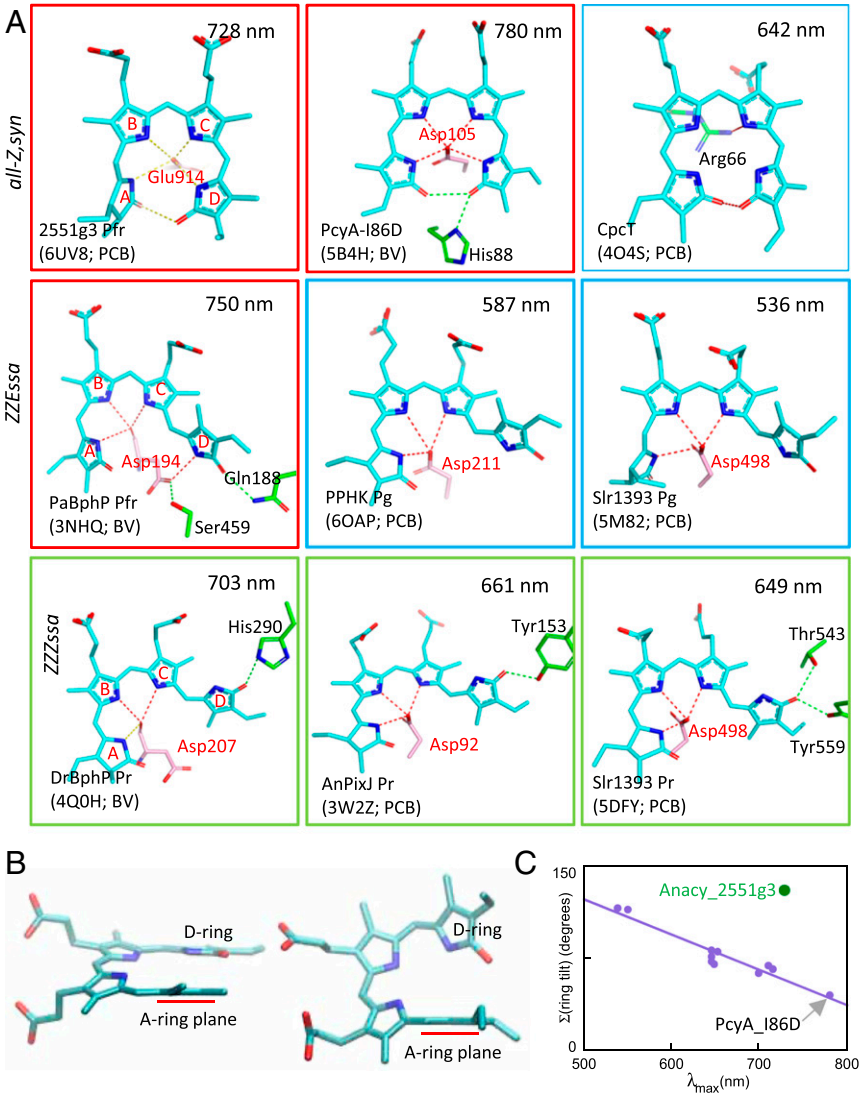

Fig. 4. Protein–chromophore interactions around D ring, bilin ring twist, and correlation with red-shifted absorption. (*A*) Direct interactions between the protein moiety and pyrrole rings within a distance of 3.5 Å are shown in dashed lines for nine representative bilin-binding structures organized according to their bilin conformations. Each panel is annotated with the bilin type (PCB or BV; in cyan) along with the corresponding PDB code and peak wavelength of the Q band absorption. In all FR-conferring structures (red outline), the ring D nitrogen directly interacts with the acidic side chain of Glu or Asp (pink) while the ring D carbonyl is hydrogen bonded to a polar moiety (green dashed lines). The green-absorbing phenotype (blue outline) correlates with the absence of the corresponding acidic residue near ring D lactam. In the red-absorbing Pr state (green outline), the ring D carbonyl is stabilized by a polar moiety while no counterion is found for the ring D nitrogen. (*B*) Side views of the *all,Z-syn* chromophores show different ring twists in PcyA and 2551g3. The bilin A and D rings in PcyA (*Left*) are much more coplanar than those in 2551g3 (*Right*). (*C*) A plot of ring tilt angles versus peak wavelength calculated using an in-house script. The sum of three angles between adjacent rings from each methine bridge was plotted against peak wavelength for several XRG CBCRs. The I_{86}D PcyA (purple; linear fit, $r^2 = 0.92$) and 2551g3 (green) are also shown for comparison.

absorption maximum at ~610 nm, whereas the PEB adducts of other phytochromes and CBCRs have absorption maxima around 560 to 570 nm (37, 72, 73). These results suggest that the conjugated A–C rings contribute to the red-shifted absorption in frCBCRs.

To determine which bilin tautomer is most probable for 2551g3 in the dark state, we examined the *2Fo-Fc* map of the *all-Z,syn* chromophore and its nearby protein environment. The map contours connecting to Glu914 are much less pronounced for A and B rings compared to those of rings C and D (Fig. 2*A*). Among the four pyrrole nitrogen atoms, the B ring nitrogen is the most distant from the counterion side chain of Glu914. This ring B nitrogen is also sandwiched between Trp916 on the β-face and the hydrophobic Leu944 on the α-face (Fig. 2*B*). Given its nonpolar environment, we propose that the B ring nitrogen is mostly deprotonated in the dark-adapted state. In a cationic bilin, three protons are thus present on other pyrrole nitrogen atoms and one must be on the oxygen atom of either the A or D ring (Fig. 5 and *SI Appendix*, Fig. S10). Such cationic lactim tautomers require the presence of H bond partners to stabilize the protonated oxygen atoms (Fig. 5 and *SI Appendix*, Fig. S10).

Upon binding to the 2551g3 apoprotein, the A and D rings of PCB are twisted out of plane in β-facial orientation due to steric compression while the twisted A ring geometry is stabilized by hydrogen bonds with the backbone moieties of Lys915 and the D ring carbonyl (Fig. 4). Based on these interactions and spectral properties, we postulate that the dark state of 2551g3 is enriched in the A ring lactim tautomer (Lactim 2 in Fig. 5) among a broad range of possible *all,Z-syn* isomers (*SI Appendix*, Fig. S10). Such a tautomer not only extends the conjugation into the A ring, but also localizes the positive charge on an terminal pyrrole, which

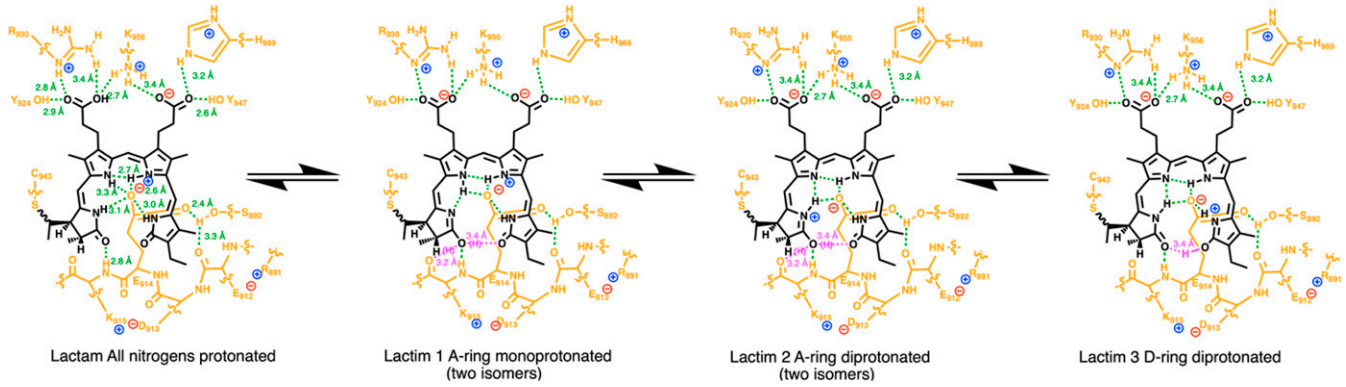

Fig. 5. Protein–chromophore interactions and bilin lactim tautomers in 2551g3. At physiological pHs, PCB in solution is neutral in the *all*-Z,*syn* configuration with two ionized propionate side chains. Upon binding to the apoprotein, both propionates form ion pairs with the cationic side chains of R930, K956, and H969 in the chromophore pocket. The A ring tilts toward the β-face as the bound chromophore engages multiple interactions with the β2–β3 loop. These include a strong H bond between the A ring carbonyl and the backbone amide NH of K915 along with protonation of the pyrrole ring system by E914. As a result, the anionic side chain of E914 forms a strong ion pair with the positively charged bilin system (Lactam All Nitrogens Protonated, *Far Left* structure). Formation of the thioether linkage via C943 may occur concomitantly or soon thereafter. Tautomerization to form Lactim 1 can occur via transient NH deprotonation, e.g., B ring NH, and proton transfer to the A ring carbonyl via the axial E914 carboxylate side chain. We envisage this A ring lactim is stabilized by H bonds with two nearby oxygen atoms, i.e., the backbone amide carbonyl of K915 and the D ring carbonyl, affording two Lactim 1 A ring deprotonated isomers. Additional tautomerization to form Lactim 2 may occur via a similar mechanism, via direct proton transfer from the B ring to the A ring pyrrole nitrogens or directly from the original Lactam. Lactim 3 can be generated by proton transfer via the A ring lactim to the D ring carbonyl. Although the positive charge can be readily delocalized on all four pyrroles, we favor an enrichment of far-red–absorbing Lactim 2 in FR/X CBCRs due to the A ring's proximity to the negatively charge β-face.

may contribute to the far-red absorption of 2551g3 (68). This proposal is also consistent with the chromophore exchange experiments indicating the role of the A ring in the red shift of 2551g3 dark state. Subtle changes in the bilin disposition caused by amino acid substitutions are expected to alter the equilibrium among tautomers (Fig. 5 and *SI Appendix*, Fig. S10), thereby resulting in spectral variations in this family of frCBCRs.

Taken together, our structural, mutational, and spectral data suggest that far-red tuning of FR/X CBCRs involves two distinct red-shifting mechanisms. Specifically, an enriched population of A ring lactim accounts for the consistent red shift observed in both *15Z* and *15E* states, and D ring protonation by a highly conserved counterion residue (Glu or Asp) contributes to the red shift associated with photoconversion. While the former appears unique to this frCBCR family, the latter is likely more general to the bilin binding proteins that utilize *15Z*/*15E* photoisomerization for light signaling. Assuming that photocycles of this family of frCBCRs utilize the same established mechanism, the primary photoproduct would be expected to adopt a *15E,syn* configuration similar to that observed in the crystal structure of the red-absorbing *15E* photoproduct state of RcaE as reported in the companion paper (65). It is reasonable to assume that the *15E* photoproduct chromophores of frCBCRs adopt similar configurations in their Pr states. The Po state, on the other hand, might arise from a trapped-twist mechanism, in which in the D ring and/or A ring are trapped in a twisted conformation in a confined chromophore pocket surrounded by bulky Trp residues. Given the high absorption ratio between the Q band and Soret band in the Po state, we therefore cannot rule out a more extended conformation for the *15E* photoproduct achieved via rotation about the C14–C15 single bond. Alternatively, photo-induced isomerization could occur via a hula twist mechanism (74), although hula twist has not been observed for bilin systems. In either case, the A ring lactim would be retained in the stable photoproducts consistent with the red shift observed for the *15E* photoproduct of 2551g3. These important questions, however, remain unresolved until the photoproduct structure is in hand. In addition, many aspects of the proposed far-red tuning mechanism call for more extensive investigation by vibrational and NMR spectroscopy as well as by excited-state calculations.

Materials and Methods

Detailed materials and methods are provided in *SI Appendix, Supplementary Methods*. This includes information on phylogenetic analysis (75, 76), cloning, expression and purification of CBCRs, spectroscopic techniques, crystallization, and structure determination.

Data Availability. The coordinates and structure factors have been deposited in the Protein Data Bank with access codes 6UVB (100 K) (77) and 6UV8 (room temperature) (78). All study data are included in the article and/or supporting information.

ACKNOWLEDGMENTS. We thank the staff at BioCARS (Center for Advanced Radiation Sources) and LS-CAT (Life Sciences Collaborative Access Team) for support in X-ray diffraction data collection at the Advanced Photon Source, Argonne National Laboratory. Use of the LS-CAT Sector 21 is supported by the Michigan Economic Development Corporation and the Michigan Technology Tri-Corridor under Grant 085P1000817. Use of BioCARS was also supported by the National Institute of General Medical Sciences under grant number NIH P41 GM118217. Use of the Advanced Photon Source is supported by the US Department of Energy, Office of Science, Office of Basic Energy Sciences, under Contract DE-AC02-06CH11357. This work is supported by grants from the US Department of Energy, Office of Science, Office of Basic Energy Sciences, under Contract E-FG02-09ER16117 to J.C.L., and from the NIH under R01EY024363 to X.Y.

1. M. Ikeuchi, T. Ishizuka, Cyanobacteriochromes: A new superfamily of tetrapyrrole-binding photoreceptors in cyanobacteria. *Photochem. Photobiol. Sci.* **7**, 1159–1167 (2008).
2. Y. Hirose *et al.*, Green/red cyanobacteriochromes regulate complementary chromatic acclimation via a protochromic photocycle. *Proc. Natl. Acad. Sci. U.S.A.* **110**, 4974–4979 (2013).
3. F. Gan *et al.*, Extensive remodeling of a cyanobacterial photosynthetic apparatus in far-red light. *Science* **345**, 1312–1317 (2014).
4. K. Fushimi, R. Narikawa, Cyanobacteriochromes: Photoreceptors covering the entire UV-to-visible spectrum. *Curr. Opin. Struct. Biol.* **57**, 39–46 (2019).
5. N. C. Rockwell, Y.-S. Su, J. C. Lagarias, Phytochrome structure and signaling mechanisms. *Annu. Rev. Plant Biol.* **57**, 837–858 (2006).
6. C. Song *et al.*, Two ground state isoforms and a chromophore D-ring photoflip triggering extensive intramolecular changes in a canonical phytochrome. *Proc. Natl. Acad. Sci. U.S.A.* **108**, 3842–3847 (2011).
7. R. Narikawa *et al.*, Structures of cyanobacteriochromes from phototaxis regulators AnPixJ and TePixJ reveal general and specific photoconversion mechanism. *Proc. Natl. Acad. Sci. U.S.A.* **110**, 918–923 (2013).
8. E. S. Burgie, J. M. Walker, G. N. Phillips Jr., R. D. Vierstra, A photo-labile thioether linkage to phycoviolobilin provides the foundation for the blue/green photocycles in DXCF-cyanobacteriochromes. *Structure* **21**, 88–97 (2013).
9. X. Yang, Z. Ren, J. Kuk, K. Moffat, Temperature-scan cryocrystallography reveals reaction intermediates in bacteriophytochrome. *Nature* **479**, 428–432 (2011).

10. X. Xu *et al.*, Structural elements regulating the photochromicity in a cyanobacteriochrome. *Proc. Natl. Acad. Sci. U.S.A.* **117**, 2432–2440 (2020).
11. S. Lim *et al.*, Correlating structural and photochemical heterogeneity in cyanobacteriochrome NpR6012g4. *Proc. Natl. Acad. Sci. U.S.A.* **115**, 4387–4392 (2018).
12. K. A. Franklin, P. H. Quail, Phytochrome functions in Arabidopsis development. *J. Exp. Bot.* **61**, 11–24 (2010).
13. J. J. Casal, Photoreceptor signaling networks in plant responses to shade. *Annu. Rev. Plant Biol.* **64**, 403–427 (2013).
14. X. Yang, J. Kuk, K. Moffat, Crystal structure of Pseudomonas aeruginosa bacteriophytochrome: Photoconversion and signal transduction. *Proc. Natl. Acad. Sci. U.S.A.* **105**, 14715–14720 (2008).
15. G. Enomoto, R. Ni-Ni-Win, R. Narikawa, M. Ikeuchi, Three cyanobacteriochromes work together to form a light color-sensitive input system for c-di-GMP signaling of cell aggregation. *Proc. Natl. Acad. Sci. U.S.A.* **112**, 8082–8087 (2015).
16. Y. Hirose *et al.*, Diverse chromatic acclimation processes regulating phycoerythrocyanin and rod-shaped phycobilisome in cyanobacteria. *Mol. Plant* **12**, 715–725 (2019).
17. L. B. Wiltbank, D. M. Kehoe, Diverse light responses of cyanobacteria mediated by phytochrome superfamily photoreceptors. *Nat. Rev. Microbiol.* **17**, 37–50 (2019).
18. G. Gourinchas *et al.*, Long-range allosteric signaling in red light-regulated diguanylyl cyclases. *Sci. Adv.* **3**, e1602498 (2017).
19. L.-O. Essen, J. Mailliet, J. Hughes, The structure of a complete phytochrome sensory module in the Pr ground state. *Proc. Natl. Acad. Sci. U.S.A.* **105**, 14709–14714 (2008).
20. J. R. Wagner, J. S. Brunzelle, K. T. Forest, R. D. Vierstra, A light-sensing knot revealed by the structure of the chromophore-binding domain of phytochrome. *Nature* **438**, 325–331 (2005).
21. E. S. Burgie, J. Zhang, R. D. Vierstra, Crystal structure of Deinococcus phytochrome in the photoactivated state reveals a cascade of structural rearrangements during photoconversion. *Structure* **24**, 448–457 (2016).
22. N. C. Rockwell, S. S. Martin, K. Feoktistova, J. C. Lagarias, Diverse two-cysteine photocycles in phytochromes and cyanobacteriochromes. *Proc. Natl. Acad. Sci. U.S.A.* **108**, 11854–11859 (2011).
23. N. C. Rockwell, S. S. Martin, A. G. Gulevich, J. C. Lagarias, Phycoviolobilin formation and spectral tuning in the DXCF cyanobacteriochrome subfamily. *Biochemistry* **51**, 1449–1463 (2012).
24. N. C. Rockwell, S. S. Martin, J. C. Lagarias, Red/green cyanobacteriochromes: Sensors of color and power. *Biochemistry* **51**, 9667–9677 (2012).
25. R. Narikawa, G. Enomoto, K. Ni-Ni-Win, K. Fushimi, M. Ikeuchi, A new type of dual-Cys cyanobacteriochrome GAF domain found in cyanobacterium Acaryochloris marina, which has an unusual red/blue reversible photoconversion cycle. *Biochemistry* **53**, 5051–5059 (2014).
26. K. Fushimi *et al.*, Cyanobacteriochrome photoreceptors lacking the canonical Cys residue. *Biochemistry* **55**, 6981–6995 (2016).
27. J. J. Tabor, A. Levskaya, C. A. Voigt, Multichromatic control of gene expression in *Escherichia coli*. *J. Mol. Biol.* **405**, 315–324 (2011).
28. A. Hueso-Gil, Á. Nyerges, C. Pál, B. Calles, V. de Lorenzo, Multiple-site diversification of regulatory sequences enables interspecies operability of genetic devices. *ACS Synth. Biol.* **9**, 104–114 (2020).
29. M. Blain-Hartung, N. C. Rockwell, J. C. Lagarias, Light-regulated synthesis of cyclic-di-GMP by a bidomain construct of the cyanobacteriochrome Tlr0924 (SesA) without stable dimerization. *Biochemistry* **56**, 6145–6154 (2017).
30. M. Blain-Hartung *et al.*, Cyanobacteriochrome-based photoswitchable adenylyl cyclases (cPACs) for broad spectrum light regulation of cAMP levels in cells. *J. Biol. Chem.* **293**, 8473–8483 (2018).
31. K. Fushimi, G. Enomoto, M. Ikeuchi, R. Narikawa, Distinctive properties of dark reversion kinetics between two red/green-type cyanobacteriochromes and their application in the photoregulation of cAMP synthesis. *Photochem. Photobiol.* **93**, 681–691 (2017).
32. P. Ramakrishnan, J. J. Tabor, Repurposing *Synechocystis* PCC6803 UirS–UirR as a UV-violet/green photoreversible transcriptional regulatory tool in *E. coli*. *ACS Synth. Biol.* **5**, 733–740 (2016).
33. S. Lim *et al.*, Photoconversion changes bilin chromophore conjugation and protein secondary structure in the violet/orange cyanobacteriochrome NpF2163g3. *Photochem. Photobiol. Sci.* **13**, 951–962 (2014).
34. N. C. Rockwell, S. S. Martin, J. C. Lagarias, Identification of DXCF cyanobacteriochrome lineages with predictable photocycles. *Photochem. Photobiol. Sci.* **14**, 929–941 (2015).
35. N. C. Rockwell, S. S. Martin, J. C. Lagarias, There and back again: Loss and reacquisition of two-Cys photocycles in cyanobacteriochromes. *Photochem. Photobiol.* **93**, 741–754 (2017).
36. T. Ishizuka *et al.*, The cyanobacteriochrome, TePixJ, isomerizes its own chromophore by converting phycocyanobilin to phycoviolobilin. *Biochemistry* **50**, 953–961 (2011).
37. N. C. Rockwell, S. S. Martin, J. C. Lagarias, Mechanistic insight into the photosensory versatility of DXCF cyanobacteriochromes. *Biochemistry* **51**, 3576–3585 (2012).
38. S. Osoegawa *et al.*, Identification of the deprotonated pyrrole nitrogen of the bilin-based photoreceptor by Raman spectroscopy with an advanced computational analysis. *J. Phys. Chem. B* **123**, 3242–3247 (2019).
39. C. Zhao, F. Gan, G. Shen, D. A. Bryant, RfpA, RfpB, and RfpC are the master control elements of far-red light photoacclimation (FaRLiP). *Front. Microbiol.* **6**, 1303 (2015).
40. N. C. Rockwell, S. S. Martin, J. C. Lagarias, Identification of cyanobacteriochromes detecting far-red light. *Biochemistry* **55**, 3907–3919 (2016).
41. K. Fushimi, M. Ikeuchi, R. Narikawa, The expanded red/green cyanobacteriochrome lineage: An evolutionary hot spot. *Photochem. Photobiol.* **93**, 903–906 (2017).
42. H. Scheer, X. Yang, K.-H. Zhao, Biliproteins and their applications in bioimaging. *Procedia Chem.* **14**, 176–185 (2015).
43. K. D. Piatkevich, F. V. Subach, V. V. Verkhusha, Engineering of bacterial phytochromes for near-infrared imaging, sensing, and light-control in mammals. *Chem. Soc. Rev.* **42**, 3441–3452 (2013).
44. J. Lecoq, M. J. Schnitzer, An infrared fluorescent protein for deeper imaging. *Nat. Biotechnol.* **29**, 715–716 (2011).
45. G. S. Filonov *et al.*, Bright and stable near-infrared fluorescent protein for in vivo imaging. *Nat. Biotechnol.* **29**, 757–761 (2011).
46. D. M. Chudakov, M. V. Matz, S. Lukyanov, K. A. Lukyanov, Fluorescent proteins and their applications in imaging living cells and tissues. *Physiol. Rev.* **90**, 1103–1163 (2010).
47. X. Shu *et al.*, Mammalian expression of infrared fluorescent proteins engineered from a bacterial phytochrome. *Science* **324**, 804–807 (2009).
48. O. S. Oliinyk, A. A. Shemetov, S. Pletnev, D. M. Shcherbakova, V. V. Verkhusha, Smallest near-infrared fluorescent protein evolved from cyanobacteriochrome as versatile tag for spectral multiplexing. *Nat. Commun.* **10**, 279 (2019).
49. K. Fushimi *et al.*, Photoconversion and fluorescence properties of a red/green-type cyanobacteriochrome AM1_C0023g2 that binds not only phycocyanobilin but also biliverdin. *Front. Microbiol.* **7**, 588 (2016).
50. K. Fushimi *et al.*, Rational conversion of chromophore selectivity of cyanobacteriochromes to accept mammalian intrinsic biliverdin. *Proc. Natl. Acad. Sci. U.S.A.* **116**, 8301–8309 (2019).
51. G. A. Gambetta, J. C. Lagarias, Genetic engineering of phytochrome biosynthesis in bacteria. *Proc. Natl. Acad. Sci. U.S.A.* **98**, 10566–10571 (2001).
52. J. Zhang *et al.*, Fused-gene approach to photoswitchable and fluorescent biliproteins. *Angew. Chem. Int. Ed. Engl.* **49**, 5456–5458 (2010).
53. Z. Ren *et al.*, Crystal-on-crystal chips for *in situ* serial diffraction at room temperature. *Lab Chip* **18**, 2246–2256 (2018).
54. Z. Ren *et al.*, An automated platform for *in situ* serial crystallography at room temperature. *IUCrJ* **7**, 1009–1018 (2020).
55. N. C. Rockwell, L. Shang, S. S. Martin, J. C. Lagarias, Distinct classes of red/far-red photochemistry within the phytochrome superfamily. *Proc. Natl. Acad. Sci. U.S.A.* **106**, 6123–6127 (2009).
56. Y. Hagiwara, M. Sugishima, Y. Takahashi, K. Fukuyama, Crystal structure of phycocyanobilin:ferredoxin oxidoreductase in complex with biliverdin IXalpha, a key enzyme in the biosynthesis of phycocyanobilin. *Proc. Natl. Acad. Sci. U.S.A.* **103**, 27–32 (2006).
57. W. Zhou *et al.*, Structure and mechanism of the phycobiliprotein lyase CpcT. *J. Biol. Chem.* **289**, 26677–26689 (2014).
58. A. Marx, N. Adir, Allophycocyanin and phycocyanin crystal structures reveal facets of phycobilisome assembly. *Biochim. Biophys. Acta* **1827**, 311–318 (2013).
59. J. Zhang *et al.*, Structure of phycobilisome from the red alga *Griffithsia pacifica*. *Nature* **551**, 57–63 (2017).
60. F. Velazquez Escobar *et al.*, Photoconversion mechanism of the second GAF domain of cyanobacteriochrome AnPixJ and the cofactor structure of its green-absorbing state. *Biochemistry* **52**, 4871–4880 (2013).
61. J. J. van Thor *et al.*, Light-induced proton release and proton uptake reactions in the cyanobacterial phytochrome Cph1. *Biochemistry* **40**, 11460–11471 (2001).
62. D. von Stetten *et al.*, Highly conserved residues Asp-197 and His-250 in Agp1 phytochrome control the proton affinity of the chromophore and Pfr formation. *J. Biol. Chem.* **282**, 2116–2123 (2007).
63. B. Zienicke *et al.*, Unusual spectral properties of bacteriophytochrome Agp2 result from a deprotonation of the chromophore in the red-absorbing form Pr. *J. Biol. Chem.* **288**, 31738–31751 (2013).
64. J. A. Rumfeldt, H. Takala, A. Liukkonen, J. A. Ihalainen, UV-vis spectroscopy reveals a correlation between Y263 and BV protonation states in bacteriophytochromes. *Photochem. Photobiol.* **95**, 969–979 (2019).
65. T. Nagae *et al.*, Structural basis of the protochromic green/red photocycle of the chromatic acclimation sensor RcaE. *Proc. Natl. Acad. Sci. U.S.A.* **118**, e2024583118 (2021).
66. Y. Hagiwara *et al.*, Atomic-resolution structure of the phycocyanobilin:ferredoxin oxidoreductase I86D mutant in complex with fully protonated biliverdin. *FEBS Lett.* **590**, 3425–3434 (2016).
67. H. Shin, Z. Ren, X. Zeng, S. Bandara, X. Yang, Structural basis of molecular logic OR in a dual-sensor histidine kinase. *Proc. Natl. Acad. Sci. U.S.A.* **116**, 19973–19982 (2019).
68. E. Maximowitsch, T. Domratcheva, A hydrogen bond between linear tetrapyrrole and conserved aspartate causes the far-red shifted absorption of phytochrome photoreceptors. *ChemRxiv* [Preprint] (2020). https:/doi.org/10.26434/chemrxiv.12278780.v1 (Accessed 1 June 2020).
69. P.-P. Peng *et al.*, The structure of allophycocyanin B from *Synechocystis* PCC 6803 reveals the structural basis for the extreme redshift of the terminal emitter in phycobilisomes. *Acta Crystallogr. D Biol. Crystallogr.* **70**, 2558–2569 (2014).
70. D. Krois, Geometry versus basicity of bilatrienes: Stretched and helical protonated biliverdins. *Monatshefte Für Chemie-Chem. Mon.* **122**, 495–506 (1991).
71. P. Singer, S. Fey, A. H. Göller, G. Hermann, R. Diller, Femtosecond dynamics in the lactim tautomer of phycocyanobilin: A long-wavelength absorbing model compound for the phytochrome chromophore. *ChemPhysChem* **15**, 3824–3831 (2014).
72. L. Li, J. T. Murphy, J. C. Lagarias, Continuous fluorescence assay of phytochrome assembly in vitro. *Biochemistry* **34**, 7923–7930 (1995).
73. Y.-F. Sun *et al.*, Orange fluorescent proteins constructed from cyanobacteriochromes chromophorylated with phycoerythrobilin. *Photochem. Photobiol. Sci.* **13**, 757–763 (2014).
74. R. S. H. Liu, Photoisomerization by hula-twist: A fundamental supramolecular photochemical reaction. *Acc. Chem. Res.* **34**, 555–562 (2001).
75. S. Q. Le, O. Gascuel, Accounting for solvent accessibility and secondary structure in protein phylogenetics is clearly beneficial. *Syst. Biol.* **59**, 277–287 (2010).
76. K. Katoh, D. M. Standley, MAFFT multiple sequence alignment software version 7: Improvements in performance and usability. *Mol. Biol. Evol.* **30**, 772–780 (2013).
77. X. Yang, Z. Ren, S. Bandara, Crystal structure of far-red-light absorbing cyanobacteriochrome at 100K. *Protein Data Bank*. https://www.rcsb.org/structure/6UVB. Deposited 1 November 2019.
78. X. Yang, Z. Ren, S. Bandara, Crystal structure of a far-red cyanobacteriochrome photoreceptor at room temperature. *Protein Data Bank*. https://www.rcsb.org/structure/6UV8. Deposited 1 November 2019.